Deep-Sea Research I 57 (2010) 284–296

Contents lists available at ScienceDirect

Deep-Sea Research I

journal homepage: www.elsevier.com/locate/dsri

The diffusive component of particulate organic carbon export in the North Atlantic estimated from SeaWiFS ocean color

Malgorzata Stramska *

Center for Hydro-Optics & Remote Sensing (CHORS), San Diego State University, 6505 Alvarado Rd., Ste. 206, San Diego, CA 92120, USA

ARTICLE INFO

Article history:
Received 18 August 2009
Received in revised form
13 November 2009
Accepted 18 November 2009
Available online 26 November 2009

Keywords:
Ocean color
Particulate organic carbon
Particulate organic carbon export
SeaWiFS

ABSTRACT

The diffusive component of the particulate organic carbon (POC) export from the ocean's surface layer has been estimated using a combination of the mixed layer model and SeaWiFS ocean color data. The calculations were carried out for several example sites located in the North Atlantic over a 10-year time period (1998–2007). Satellite estimates of surface POC derived from ocean color were applied as an input to the model driven by local surface heat and momentum fluxes. For each year of the examined period, the diffusive POC flux was estimated at a 200 m depth. The highest flux is generally observed in the spring and fall seasons, when surface waters are weakly stratified. In addition, the model results demonstrate significant interannual and geographical variability of the flux. The highest diffusive POC flux occurs in the northern North Atlantic and the lowest in the subtropical region. The interannual variability of the diffusive POC flux is associated with mixed layer dynamics and underscores the importance of atmospheric forcing for POC export from the surface layer to the ocean's interior.

1. Introduction

The fixation of inorganic carbon into organic matter in the photic zone, its transformation by food web processes, and subsequent vertical transport by physical mixing and gravitational settling of particles are commonly called the biological pump (e.g., Ducklow et al., 2001). Determining the efficiency of the biological pump, including the magnitude of the fraction of primary production (PP) that is removed from the euphotic zone (export production, e.g., Dugdale and Goering, 1967; Eppley and Peterson, 1979; Eppley, 1989) has been a high priority research objective in oceanography, because of its potential significance for the atmospheric CO_2 budget and global climate.

Over the years a number of methods have been used to estimate particulate organic carbon (POC) export from surface waters to greater depths. The experimental techniques include direct measurements of vertical particulate fluxes with moored or drifting sediment traps (e.g., Martin et al., 1993; see also reviews by Antia et al., 2001; Berelson, 2001; Lutz et al., 2002; Honjo et al., 2008) and the application of naturally occurring radionuclides, for example thorium-234 (^{234}Th), as tracers for sinking particles (e.g., Buesseler et al., 1992, 1995). The modeling approaches for estimating the strength of the biological pump include food web and particle transformation models (e.g., Legendre and Rivkin, 2002; Boyd and Stevens, 2002), ecosystem models (e.g., Patsch et al., 2002; Lima and Doney, 2004), and inverse models of biogeochemical processes based on distributions of oxygen, dissolved nutrients, and carbon in the ocean (Anderson et al., 2000; Schlitzer, 2004; Schlitzer et al., 2003; Usbeck et al., 2003). Approaches in which primary and export production are estimated from chlorophyll distributions obtained from ocean color satellite data have also been developed (e.g., Antoine et al., 1996; Behrenfeld and Falkowski, 1997; Behrenfeld et al., 2005; Laws et al., 2000; Dunne et al., 2007). In comparison to in situ measurements, which are usually limited geographically and temporally, satellite and modeling methods have the advantage of providing export estimates for extended periods of time for large regional, basin, and global scales. Unfortunately, all current POC flux estimates involve substantial uncertainties for a variety of reasons. For example, satellite estimates of export production rely on assumed conversion of chlorophyll *a* concentration (Chl) to productivity rates, phytoplankton Chl/POC ratios, and export production ratios (*f*), which are hard to quantify accurately and validate with a limited number of in situ calibration sites. A number of issues relating to sediment trap efficiency remain unresolved (e.g., Siegel and Deuser, 1997; Siegel et al., 2008). Inverse model calculations suggest higher estimates of POC fluxes from surface to mid-water depths than sediment trap and satellite-based methods (Schlitzer, 2004; Usbeck et al., 2003). The uncertainties inherent in the current POC flux estimates indicate a need for further development of alternative ways for studying POC dynamics and fluxes in the ocean.

* Corresponding author. Tel.: +1 619 594 2229; fax: +1 619 594 8670.
E-mail addresses: mstramska@ucsd.edu, mstramska@chors.sdsu.edu (M. Stramska).

0967-0637/$ - see front matter © 2009 Elsevier Ltd. All rights reserved.
doi:10.1016/j.dsr.2009.11.007

In this paper, satellite ocean color data and a mixed layer model are used to derive estimates of the diffusive component of the POC export flux (PE_d) at seven sites in the North Atlantic. This diffusive component accounts for that fraction of the total POC export (PE), which is transported by vertical turbulent mixing out of the oceanic surface waters. One of the goals of this paper is to demonstrate that PE_d contributes significantly to total POC export. In addition we would like to develop a basic understanding of the geographical and temporal (seasonal and interannual) variability of PE_d in the North Atlantic and its responses to atmospheric forcing. Note that, traditionally, transport by the zooplankton (particularly by the diel migrators) and gravitational settling of biogenic aggregates ballasted by heavy biomineral and lithogenic particles have been considered as the two basic processes influencing PE (e.g., Honjo et al., 2008). The role of POC export by the vertical mixing has not received much attention, while our calculations indicate that PE_d is significant for the initial transport of particles from surface waters to below the mixed layer.

2. Study sites

The geographical locations of the seven sites discussed in this paper are displayed in Fig. 1. These sites are meant to represent different biogeochemical provinces in the North Atlantic (Longhurst, 1998). Each site corresponds to an open ocean region where historical oceanographic data sets provide a context for our results. The sites are briefly presented below.

2.1. Site #1 (31°40′N 64°10′W)

This site is located near Bermuda, in the western North Atlantic subtropical gyre province (NAST-W, Longhurst, 1998). Multiyear in situ oceanographic and biogeochemical data sets are available from Hydrostation S, the Bermuda Atlantic Time-series Study (BATS; Michaels and Knap, 1996; Steinberg et al., 2001; Lomas and Bates, 2004), as well as the Ocean Flux Program (OFP, e.g., Deuser, 1986; Conte et al., 2001, 2003). Primary productivity (PP) at the BATS site displays high seasonal variability with maximum daily rates observed during the winter/spring convective mixing period. During this time, the mixed layer depth (MLD) is 200 m deep and elevated nutrients are available in the euphotic zone. In the summer, PP is limited by nutrients (e.g., Steinberg et al., 2001). Annual net PP at this site has been estimated at about 360 mg C m^{-2} day^{-1} (Michaels et al., 1994). Particulate flux is characterized by a strong seasonal cycle. There is significant interannual variability in the timing, duration, and magnitude of the seasonal peak flux. In addition, abrupt short-lived peaks in mass flux in December–January have been reported (Conte et al., 2001).

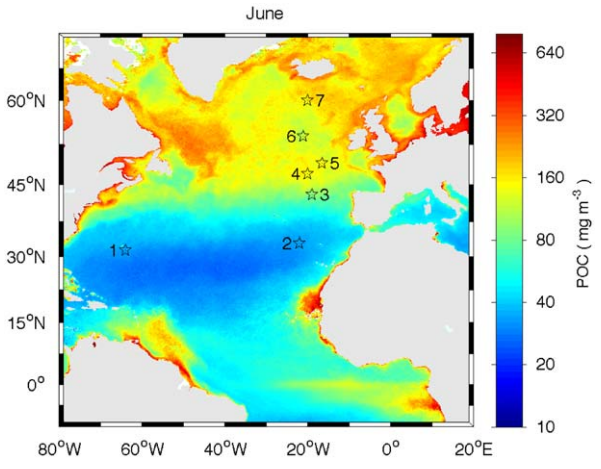

Fig. 1. Map of the 10-year averaged (1998–2007) monthly mean surface POC concentration derived from SeaWiFS for the month July, showing the location of the study sites used in this paper.

2.2. Site #2 (33°N 22°W)

This site is located west of Madeira in the eastern part of the North Atlantic Subtropical Gyral Province (NAST-E, Longhurst, 1998). Long-term observations of carbon fluxes and other oceanographic parameters at this site have been part of the German Joint Global Ocean Flux Study (JGOFS) program (station L1/K276, e.g., Waniek et al., 2005a,b). Other data sets from NAST-E province include data from the European Union Canary Islands Azores Gibraltar Observations Project (CANIGO) and from the European Station for Time Series in the Ocean, Canary Islands (ESTOC), located at 29°10′N, 15°30′W (e.g., Neuer et al., 2002, 2007).

This region is influenced by the Azores Current, which is an extension of the Gulf Stream. The winter mixing of the waters is relatively weak (100–200 m). The MLD stratification to 20–40 m occurs in March (Waniek et al., 2005a). PP is estimated at about 370 mg C m^{-2} day^{-1} (Dunne et al., 2007), and is limited by nutrients. For example, nitrate is only available in surface waters when the mixed layer is at its deepest, with concentrations of less than 1.0 μM, (Glover and Brewer, 1988; Waniek et al., 2005a). Surface chlorophyll *a* concentrations are about 0.5 mg m^{-3} during February and smaller than 0.2 mg m^{-3} during summer. The maximum particulate flux in deep-water moored sediment traps was documented in February, while a minimum flux occurred between April and August (Waniek et al., 2005b). Interestingly, particulate flux measured at ESTOC (NAST-E province) has been lower by a factor of up to four than the flux documented at BATS (NAST-W province), despite similar annual primary production at both sites (Neuer et al., 2007).

2.3. Site #3 (43°N 19°W)

This site represents a transition zone between productive regions in the north, associated with deep winter mixed layers (500 m and more), and oligotrophic regions in the south, associated with shallower (100–200 m) winter mixed layers (de Boyer Montégut et al., 2004). The site at 43°N 19°W is characterized by a pronounced seasonal cycle, and significant year-to-year variability. Data collected during the Programme Ocean Multidisciplinaire Meso Echelle (POMME) research project (Memery et al., 2005) indicate that MLD during late winter is highly variable due to day-to-day changes in the air–sea heat fluxes. The onset of the spring bloom is coincident with the rapid shallowing of the MLD, which takes place from mid-March through early May. The maximum Chl observed during POMME was about 1 mg m^{-3}. Interannual variability over the POMME area, including bloom timing and intensity, is caused by the variable position of the geographical frontier between subpolar, midlatitude and subtropical regimes (Levy et al., 2005). Primary productivity, estimated at 677 mg C m^{-2} day^{-1} (Dunne et al., 2007), is in summer limited by nutrients. Sediment trap data from the POMME region documented a clear seasonal cycle and significant interannual variability of particulate flux. Seasonal peak flux was observed in March–April in 2001, while in 2002 it was documented in April–May. This peak flux was significantly higher in 2001 (Guieu et al., 2005).

2.4. Sites #4 (47°N 20°W) and #5 (49°N 16.5°W)

These sites are located in the temperate latitudes of the North Atlantic Drift Region (NADR, Longhurst, 1998). Site #4, located at 47°N 20°W, corresponds to station L2 of the German JGOFS program (Waniek et al., 2005b). Site #5, positioned at 49°N 16.5°W, represents the location of deep sediment trap moorings deployed during the Porcupine Abyssal Plain (PAP) study within the European Union project BENGAL (high-resolution temporal and spatial study of the BENthic biology and Geochemistry of a northeastern Atlantic abyssal Locality, e.g. Lampitt et al., 2001). In addition, this region was investigated during the 1989 JGOFS North Atlantic Bloom Experiment (NABE), and there is considerable background information on the upper ocean processes (see DSR special volume 40: 1/2, 1993). The region is under the influence of the North Atlantic Current and the southward recirculation of the subtropical gyre. The winter mixed layer is deep (300–500 m) with high nutrient concentrations (e.g. 6–8 μM of nitrate, Waniek et al., 2005b). A significant increase of phytoplankton concentration (above 4 mg m^{-3}) occurs between April and May. In late summer the surface waters are nutrient-limited, and Chl decreases (<1 mg m^{-3}). The annual primary production is about 750 mg C m^{-2} day^{-1} (e.g. Dunne et al., 2007). Deep-water moorings at this site show seasonal maximum in the POC flux in February–March and another, less pronounced increase in the flux in August. Data collected during NABE (Buesseler et al., 1992) demonstrate the occurrence of episodic pulses of POC export in the early spring.

2.5. Site #6 (54°N 21°W)

This study site, located at the boundary between NADR and the Atlantic Subarctic (SARC, Longhurst, 1998) provinces, is under the direct influence of the branches of the North Atlantic Current (NAC). The winter MLD is typically 300–500 m deep, and there is enough light to support phytoplankton growth only during a relatively short period of time in spring and summer. Annual primary production has been estimated at about 700 mg C m^{-2} day^{-1} (Dunne et al., 2007). In this region, the spring bloom starts to the north and east of Iceland in March, and subsequently develops throughout the region in the following months. Chl varies between 0.6 and 1.5 mg m^{-3} from April through September. Sediment traps located at 2000 m depth recorded highest POC flux during summer (Waniek et al., 2005b).

2.6. Site #7 (60°N 20°W)

This site is located in the Subarctic North Atlantic (SARC), a region with strong seasonal signal in physical and biogeochemical properties. Historical data are available from this region from Ocean Weather Stations India and Lima, and from Marine Light in Mixed Layer (MLML) study carried out in 1989 and 1991 (e.g., Dickey et al., 1994; Plueddemann et al., 1995). The conditions at this site can be summarized as follows. The extremely deep winter mixed layer ($\sim$700 m) is caused by a combination of convective cooling and wind mixing. The April–May period is a time of transition, when ML shoals in response to increasing surface radiation and decreasing wind stress. Phytoplankton blooms are intense with Chl as high as 5 mg m^{-3}, annual PP has been estimated at about 550 mg C m^{-2} day^{-1} (Dunne et al., 2007). Mooring data from MLML experiment documented short pulses of organic matter being diluted from surface waters during the initial phase of the phytoplankton bloom, in response to atmospheric forcing (Plueddemann et al., 1995; Stramska et al., 1995).

3. Data and methods

In our approach, the surface POC concentrations estimated from satellite imagery were used as the input to a physical mixed layer model. The model allowed us to simulate the effects of physical forcing on POC dynamics and export from the oceanic surface layer, assumed in our study as the top 200 m layer of water. Note, that our method is based on a direct assessment of POC concentration from ocean color; therefore there is no need for any assumptions about the relationships between Chl and PP or Chl and POC concentration. Meteorological data were used as surface boundary conditions for the mixed layer (ML) model, as described below. Although the results are presented for selected seven example sites in the North Atlantic, our methodology is general and applicable to other geographical locations.

3.1. Model description

Our calculations are based on the one-dimensional (1D) version of the level 2.5 Mellor–Yamada (MY) mixed layer model (Mellor and Yamada, 1974, 1982; Blumberg and Mellor, 1983; see also Mellor, 2004). This model belongs to the class of differential ML models. In contrast to integrated ML models, the MY model enables a computation of vertical profiles of turbulent variables and includes realistic, stability-dependent eddy diffusivity coefficients. These features of the model are useful for simulations of the influence of local atmospheric forcing on POC export.

Basic equations of the MY model (see Mellor, 2004 for details) are given below, for a quick reference. The model solves the turbulent forms of the momentum and thermodynamic equations with some simplifying assumptions for closing the system. For a horizontally homogenous ocean with no mean vertical water motion, the equations of conservation of momentum and heat can be written as follows:

$$\frac{\partial U}{\partial t} - f(V - V_g) = \frac{\partial}{\partial z}\left[(K_M + \nu_M)\frac{\partial U}{\partial z}\right]$$

$$\frac{\partial V}{\partial t} - f(U - U_g) = \frac{\partial}{\partial z}\left[(K_M + \nu_M)\frac{\partial V}{\partial z}\right] \quad (1)$$

$$\frac{\partial T}{\partial t} = \frac{\partial}{\partial z}\left[(K_H + \nu_H)\frac{\partial T}{\partial z}\right] + \frac{1}{\rho_0 c_p}\frac{\partial I}{\partial z}$$

where t is the time, z the vertical coordinate, U and V the mean horizontal velocity components, T the mean water temperature, I the irradiance, f the Coriolis parameter, K_M and K_H the eddy coefficients for vertical turbulent diffusion, ν_M and ν_H the coefficients for molecular and background diffusion, ρ_o the water density, and c_p the specific heat of water. For simplicity, the geostrophic current components U_g and V_g are taken to be zero. The equation set (1) is closed using the following formulas for the eddy coefficients:

$$K_M = lqS_M \quad (2)$$

$$K_H = lqS_H$$

where l is the turbulent length scale, $q^2/2$ the turbulent kinetic energy, and S_M and S_H are stability functions dependent on the local Richardson number. The temporal evolution of the vertical profiles of POC concentration is described by adding the following equation to set (1):

$$\frac{\partial \mathrm{POC}}{\partial t} = \frac{\partial}{\partial z}\left[(K_H + \nu_H)\frac{\partial \mathrm{POC}}{\partial z} - (w\mathrm{POC})\right] - L \cdot POC \quad (3)$$

where w is the particle gravitational settling velocity and L the remineralization rate (taken as 0.1 day^{-1}, e.g. Edwards, 2001).

This description of POC dynamics is based on the following assumptions. First, POC particles do not affect hydrodynamic processes within the mixed layer. Second, the same diffusivity coefficient as for other scalar quantities such as salinity and heat also applies to POC. This assumption is at present necessary as no information is available about the diffusivity coefficient for POC in the ocean. Note that similar assumptions are commonly used in models simulating phytoplankton dynamics in the ocean (e.g., Fasham et al., 1990; Marra and Ho, 1993; Kantha, 2004). Finally, a constant particle gravitational settling velocity (w) equal to 2 m day^{-1} is assumed in the calculations. At present there is a significant uncertainty regarding the exact particle sinking velocities within the mixed layer, but a value of about 2 m day^{-1} is often assumed in ecosystem models (e.g., Huisman et al., 1999). To investigate the sensitivity of the model to the uncertainties in w, additional calculations with w=0 and 4 m day^{-1} were also carried out.

For the numerical calculations, Eqs. (1) and (3) were transformed into finite difference equations. Because we are interested in the diffusive POC flux out of the surface layer (defined here as the top 200 m layer of the ocean), the vertical grid spacing has been optimized to obtain higher vertical resolution near the surface. The distance between computational grid points increased with depth according to a geometrical progression. The interval was 1 m at the surface and about 5.6 m at the deepest level, and there were 400 levels down to a depth of 1082.9 m. The time step was set to 10 min. The diffusive component of the POC flux discussed in this paper is described by the first term in the brackets on the right-hand side of Eq. (3) and is interpreted as that portion of the total POC flux that is exported from surface waters by turbulent mixing.

3.2. Meteorological forcing

The meteorological data from the NOAA-CIRES Climate Diagnostic Center NCEP/NCAR (National Centers for Environmental Prediction and National Center for Atmospheric Research) Reanalysis 2 were applied to parameterize the atmospheric forcing used to run the mixed layer model. The Reanalysis Project employs a state-of-the-art analysis/forecast system to assimilate global meteorological data from various available sources from 1948 to the present. In particular, the 6 h averaged zonal and meridional wind stress components, the net latent, net long-wave, and sensible heat fluxes, as well as the net short-wave radiation flux estimates were used to establish surface boundary conditions for the model at each North Atlantic location selected for our study. In the model runs, the net heat loss, calculated as the sum of the net latent, net long-wave, and sensible heat fluxes, was applied at the sea surface. The short-wave radiation flux was assumed to penetrate into the water column and to act as the internal heat source. The absorption of solar radiation was calculated according to Paulson and Simpson (1977) for class I waters, corresponding to open ocean waters (Jerlov, 1968). Note that for simplicity our version of the model assumes a null salinity flux at the ocean surface, i.e., the model does not account for changes in the water salinity due to sea ice processes, evaporation, and precipitation. The latent heat of evaporation is included in the calculations of the net heat flux.

3.3. Surface POC concentrations

Surface POC concentrations were derived from ocean color data collected with the SeaWiFS (Sea-viewing Wide Field-of-view Sensor) instrument over a period of 10 years from 1998 through 2007. These POC estimates were calculated from Level 3 binned daily normalized water leaving-radiances, $L_{wn}(\lambda)$, with a nominal 9 km × 9 km resolution (reprocessing version 5.2). Recall that the standard NASA data processing procedures used to derive L_{wn} involve atmospheric corrections and removal of pixels with land, ice, clouds, heavy aerosol load, or negative values of retrieved radiances (e.g., Gordon and Wang, 1994; Campbell et al., 1995; IOCCG, 2004). In this study, the normalized water-leaving radiances at 443, 490, and 555 nm were used. These data were obtained from the NASA Ocean Color FTP site (http://oceancolor.gsfc.nasa.gov/ftp.html).

Methods to derive surface POC concentrations were the same as described by Stramska (2009). First, the $L_{wn}(\lambda)$ data were converted to remote sensing reflectances, $R_{rs}(\lambda)$, using the following relationship (e.g. Mobley, 1994):

$$R_{rs}(\lambda) = L_{wn}(\lambda)/F_0(\lambda) \quad (4)$$

where λ indicates the spectral waveband, $R_{rs}(\lambda)$ the spectral remote sensing reflectance in sr^{-1}, $L_{wn}(\lambda)$ the normalized water leaving radiance in μW cm^{-2} nm^{-1} sr^{-1}, and $F_0(\lambda)$ the extra-terrestrial solar irradiance taken as $F_0(443)$=190.154, $F_0(490)$=196.473, and $F_0(555)$=183.010 in μW cm^{-2} nm^{-1}. The $F_0(\lambda)$ values, derived by averaging the Thullier spectrum at the nominal wavelengths of SeaWiFS, were made available by NASA (http://oceancolor.gsfc.nasa.gov/DOCS/RSR_tables.html). In the next step, the remote sensing reflectances were used to calculate daily surface POC concentrations, using algorithms summarized in Table 1. For full details on the methods used to derive the POC algorithms please refer to the original paper by Stramski et al. (2008). In summary, these algorithms are based on the relationships established from *simultaneous* collection of water samples for POC determinations and in situ measurements of $R_{rs}(\lambda)$. This means that these POC algorithms are based on a similar philosophy as has been developed over the years by the ocean color community to construct ocean color *Chl* algorithms (e.g., O'Reilly et al., 1998, 2000). Importantly, the data sets used to derive the POC algorithms covered provinces from hyper-oligotrophic and oligotrophic waters within subtropical gyres to eutrophic coastal upwelling regimes, therefore the algorithms have been recommended for application in a broad range of oceanic conditions.

In our calculations both algorithms listed in Table 1 have been used and our final estimates of surface POC concentrations are based on averaging the results from the two algorithms (Stramska, 2009). Calculations always started with deriving the daily fields of POC concentrations, because our POC algorithms are nonlinear. From daily POC imagery, we calculated 21-day moving

Table 1
Summary of the POC band-ratio algorithms used in this paper.

$$POC = A_i[R_{rs}(\lambda)/R_{rs}(555)]^{-Bi}$$

$R_{rs}(\lambda)/R_{rs}(555)$	A_i	B_i	R^2	*RMSE* (mg m^{-3})	*MNB* (%)	*NRMS* (%)	*N*
$R_{rs}(443)/R_{rs}(555)$	203.2	1.034	0.871	21.29	2.26	21.68	53
$R_{rs}(490)/R_{rs}(555)$	308.3	1.639	0.906	18.38	2.28	21.71	52

The $R_{rs}(\lambda)/R_{rs}(555)$ is the blue-to-green band ratio of remote sensing reflectance, POC is in mg m^{-3}, and A_i and B_i are regression coefficients, fitted by least-squares linear regression analysis using $\log_{10}$-transformed data of POC and $R_{rs}(\lambda)/R_{rs}(555)$. All regression coefficients and statistical parameters have been recalculated to represent the non-transformed data. The light wavelength λ is either 443 or 490, R^2 is the determination coefficient, *RMSE* the root mean square error, *MNB* the mean normalized bias, *NRMS* the normalized root mean square error, and *N* the number of observations (see Stramski et al., 2008 for more details).

averages to fill in the missing data. Finally, the 21-day averaged POC concentrations were binned within $2^\circ \times 2^\circ$ cells centered on each study site, to filter out smaller scale variability. Note that gaps in the time series due to missing data were still present after this spatial and temporal averaging in the northern regions in winter.

3.4. Model runs

Model calculations were carried out for each of the seven sites described in Section 2. The heat fluxes and wind stress data were interpolated linearly to provide 10 min temporal resolution data appropriate for the time step used in the model. Similarly, the surface POC data were interpolated with the same time resolution until the last daily POC data available in the year. In the northern North Atlantic (i.e. at sites at 49°N, 54°N, and 60°N), during winter, satellite ocean color data were missing (i.e. due to frequent clouds). When this was the case, the surface POC concentration at the end of the calendar year was adjusted in the model, by assuming that internal POC sources within the mixed layer were equal to zero (no production). This means that POC was gradually diluted when ML was deepening. If the data were also missing in January, the POC concentration at the beginning of the year was filled in by the liner interpolation of the data between the end of the previous year and the first available data in a given year (in January or February). Thus, it is important to understand that the PE_d estimates in the northern sties (in particular at 54°N and 60°N) include this additional source of uncertainty in winter in comparison to other sites, caused by the missing ocean color data.

Initial profiles of water temperature, salinity and POC concentration used to start the calculations at a given geographical location were assumed to be the same for all years. Initial POC was taken to be homogenous throughout the water column and equal 20 mg m^{-3} at all sites. Initial temperature and salinity profiles were taken from the World Atlas 2005 climatology (http://www.nodc.noaa.gov/OC5/SELECT/woaselect/woaselect.html) for the month of December at the geographical position nearest to each site. During all model runs, the water temperature, salinity, and POC concentration at the deepest grid point of the model were assumed to be constant. The Bermuda Atlantic Time Series (BATS) site (31°40′N 64°10′W) is the only location where time series of deep-water POC concentration are available. At BATS, the POC concentrations close to the assumed value of 20 mg m^{-3} were observed at 1000 m depth in 2000–2002 (see http://bats.bbsr.edu). Similar values of deep-water POC concentrations were measured during our cruises in the North Atlantic (unpublished data). In each case the model was run for 10 days for a spin-up using meteorological data from December of the previous year. The results from these 10-day runs have not been included in the further analysis of the model results. Yearly time series of the diffusive POC export reported in this paper are based on a full year of model run following the initial spin-up.

3.5. Other data

The initial profiles of the water temperature and salinity were taken from World Atlas 2005 climatology provided by NOAA (http://www.nodc.noaa.gov/OC5/SELECT/woaselect/woaselect.html). The monthly climatological mixed layer depth (MLD) data were made available by the Laboratoire d'Océanographie Dynamique et de Climatologie, Université Pierre et Marie Curie in Paris (de Boyer Montégut et al., 2004). POC flux data from open ocean sites in the Atlantic have been compiled from existing literature for comparisons with PE_d derived in this paper (Table 2). We have also used PP and PE estimates kindly provided by John Dunne (personal communication) for comparisons with the calculated PE_d estimates. The PP and PE estimates have been derived from 1998 to 2004 SeaWiFS data (Dunne et al., 2007). The primary productivity estimates used in our paper represent an average of PP obtained by Dunne et al. (2007) from three algorithms described by Behrenfeld and Falkowski (1997), Carr (2002), and Marra et al. (2003).

In the final paragraph discussing the results we recommend that, in the future, atmospheric forcing should be taken into account when experimental data on POC export are analyzed. This could be done without running complex ocean models, but using simple correlations based on bulk mixed layer theories (Kraus and Turner, 1967; Niiler and Kraus, 1977; Follows and Dutkiewicz, 2002). According to these theories, vertical mixing of water properties in the vertically homogenous oceanic mixed layer is related to the rate of generation of turbulent kinetic energy (TKE_{RT}). The TKE_{RT} can be quantified in terms of wind stirring and buoyancy forcing

$$TKE_{RT} = m_1 u_*^3 + m_2 \frac{\alpha g}{\rho c_p} \frac{MLD}{2} (-H_0) \quad (5)$$

where TKE is the turbulent kinetic energy, MLD the mixed layer depth, u_* the wind-induced friction velocity, ρ the water density, c_p the specific heat, g the gravitational acceleration, α the coefficient of logarithmic expansion of ρ as a function of water temperature, and H_0 the net heat flux. The coefficients m_1 and m_2 have been assumed $m_1=1.25$ and $m_2=1$ for negative buoyancy forcing (heat loss from the surface ocean) and $m_2=0.2$ for positive buoyancy forcing (surface ocean gains heat) (e.g., Kraus et al., 1988). Eq. (5) estimates the TKE_{RT} with the assumption that effects due to internal waves, energy dissipation, and variable vertical distribution of penetrative radiation with water turbidity are small and can be neglected. The first term on the right-hand side of Eq. (5) ($m_1 u_*^3$) represents the rate of work by the wind. The second term on the right-hand side of Eq. (5) ($m_2((\alpha g/\rho c_p)(MLD/2))(-H_0)$) describes the rate of potential energy change produced by heat fluxes across the ocean surface. Note that the wind action always increases TKE_{RT} in the oceanic boundary layer. The buoyancy forcing can either increase TKE_{RT} when the water column is cooled from above ($H_0 < 0$), or reduce TKE_{RT} when the water column is stratifying due to heat input to the surface ocean from the atmosphere ($H_0 > 0$). Eq. (5) could be easily applied for investigating the relationship between in situ POC export and meteorological data without running complex ocean models. To stress this point we have included in the results section a correlation plot between TKE_{RT} and PE_d.

4. Results and discussion

The application of our model to a 10-year long record of satellite-derived POC estimates reveals patterns of regional, seasonal and interannual variability of the vertical diffusive POC flux (PE_d) in the North Atlantic sites. We discuss here the diffusive flux PE_d at 200 m depth estimated with model runs using a constant particle gravitational settling velocity, $w=2$ m day^{-1}. Additional calculations with $w=0$ and $w=4$ m day^{-1} yield very similar ($\pm 2\%$) estimates of the diffusive POC flux at 200 m depth; therefore, the results from these model runs are not presented here.

The example model inputs (net heat flux, wind stress magnitude, and surface POC concentration) and calculated PE_d are displayed in Figs. 2–5. These data represent four study sites (located at 31°40′N 64°10′W, 33°N 22°W, 47°N 20°W, and 54°N 21°W), and correspond to the following biogeochemical provinces

Table 2
Comparison of model-derived diffusive POC flux with estimates of POC flux ($mg\,m^{-2}\,day^{-1}$) from literature.

Site	Model derived PE_d	PE from Dunne et al. (2007)	PE from in situ data	In situ location	References for in situ data
60°N 20°W	41.3–83.6	165.4	460	65.5°N 0.1°W	Honjo and Manganini (1987) Honjo et al. (2008)
54°N 21°W	44.8–112.1	212.8	250	54.7°N 21.2°W	Scholten et al. (2001)
			235	54.5°N 21.1°W	Scholten et al. (2001)
49°N 16.5°W	31.0–74.1	203.3	130	49.1°N 13.4°W	Scholten et al. (2001)
			280	34–48°N 21–22°W	Lutz et al. (2002)
47°N 20°W	41.0–77.6	198.6	65–85	47.8°N 19.5°W	Honjo et al. (2008)
			280	34–48°N 21–22°W	Lutz et al. (2002)
43°N 19°W	6.6–38.6	159.1	50.0	43°N 19°W	Guieu et al. (2005)
33°N 22°W	0.0–10.2	43.8	46.0	33°N 22°W	Scholten et al. (2001)
			7.0	29°10′N 15.5°W	Neuer et al. (2007)
31°40′N 64°10′W	1.3–36.4	29.9	33.0–40.0	31°40′N 64°10′W	Lutz et al. (2002)

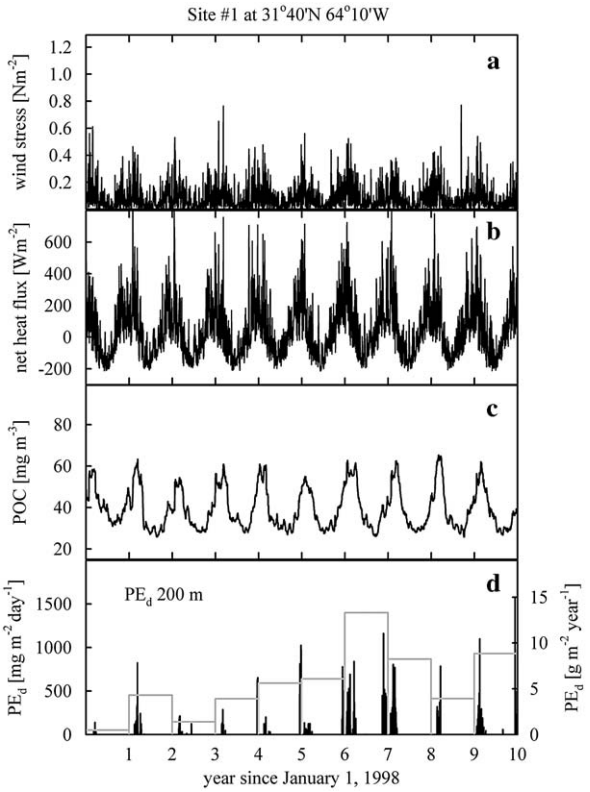

Fig. 2. Example time series of (a) wind stress magnitude, (b) net heat flux, and (c) ocean color-derived surface POC concentration at site #1 (31°40′N 64°10′W) used as an input to the model. (d) Model estimated diffusive POC export. Daily time series are shown as black solid line and yearly totals are shown as gray histogram. The vertical scales on the left and right sides of plot (d) are for daily time series and yearly estimates of PE_d, respectively.

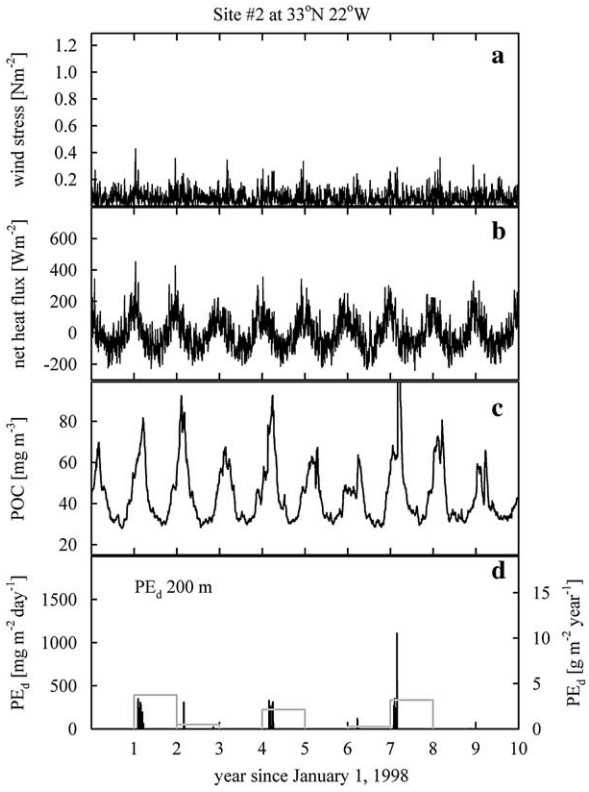

Fig. 3. Same as in Fig. 2, but for site #2 (33°N 22°W).

in the northeast Atlantic: NAST-W, NAST-E, the North Atlantic Drift Region (NADR), and the southern boundary of the Subarctic Province (SARC). A comparison of the calculated 10-year time series of PE_d at all seven study sites investigated in this paper is presented in Fig. 6. The annual average PE_d values (in $g\,m^{-2}\,year^{-1}$) are shown as histograms, and compared with the 10-year time series of the daily PE_d estimates (in $mg\,m^{-2}\,day^{-1}$). Note that the vertical scales for PE_d are the same for all sites shown in Fig. 6, to stress the differences between the sites. These results underline regional and interannual differences regarding the intensity of the PE_d. In general, the PE_d estimates are larger in the northern regions and decrease to the south. The largest annual PE_d (above $40\,g\,m^{-2}\,year^{-1}$) is estimated for the SARC site at 54°N in year 2000. The PE_d can be as high as about $30\,g\,m^{-2}\,year^{-1}$ at sites at 60°N 20°W, 49°N 16.5°W, and 47°N 20°W, but is always less than $20\,g\,m^{-2}\,year^{-1}$ at the site at 43°N and south. The lowest PE_d estimate is associated with the site at 33°N 22°W (NAST-E). The BATS site at 31°40′N, 64°10′W (NAST-W) is characterized by a significantly higher estimate of PE_d than the NAST-E site at 33°N 20°W, which is most likely related to a larger amplitude of the yearly net heat cycle and larger magnitude of wind stress observed at BATS site than at the NAST-E site (compare Figs. 2 and 3). Such differences in atmospheric forcing result in less energetic mixing of surface waters in the NAST-E region. Note that the average PE_d is larger at BATS site, in spite of the fact that on average the surface POC concentrations used to run the model reached higher values at the NAST-E site. Observe also that there is a significant interannual variability in PE_d at all sites. For example at 54°N the maximum PE_d is observed in year 2000 and the minimum is estimated for 1998. At 47°N the maximum PE_d is calculated for 1999 and the minimum for 2007, while at BATS site maximum PE_d is observed in year 2000.

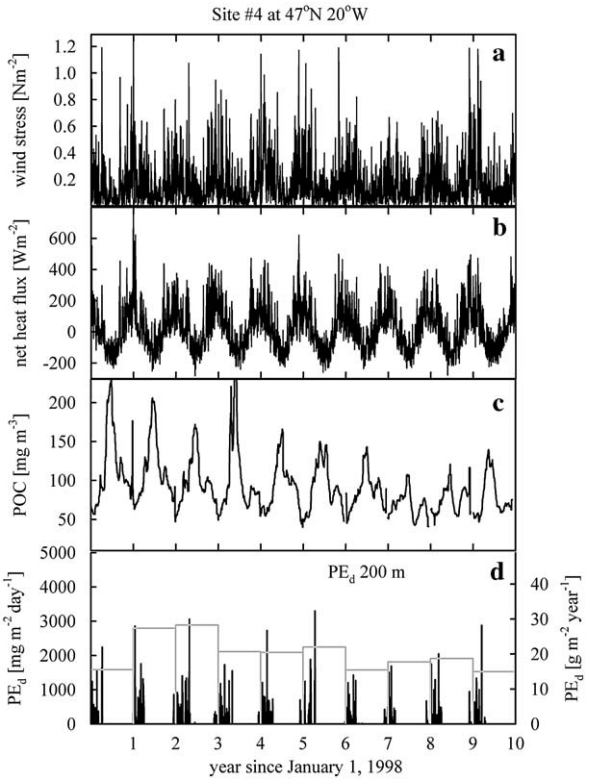

Fig. 4. Same as in Fig. 2, but for site #4 (47°N 20°W).

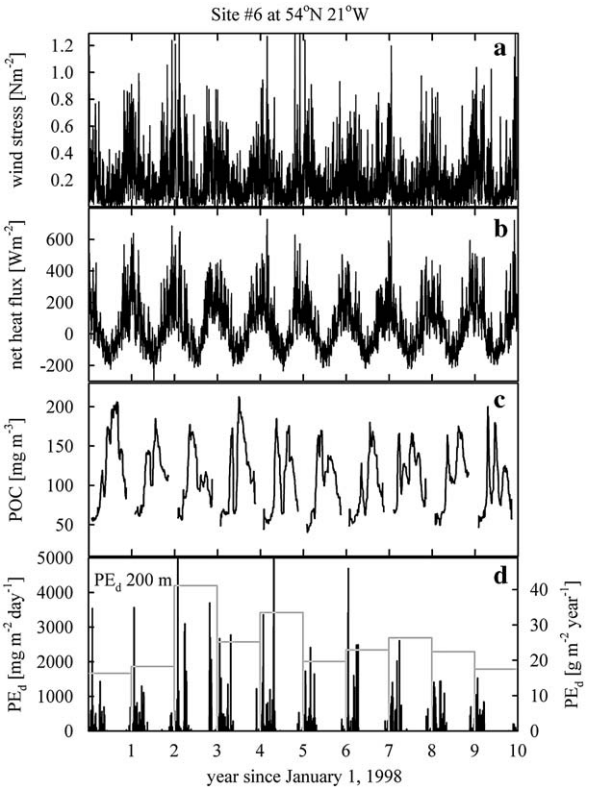

Fig. 5. Same as in Fig. 2, but for site #6 (54°N 21°W).

To better visualize the seasonal trends, time series of the 10-year averaged PE_d estimates are plotted for each of the seven sites in Fig. 7, together with the mixed layer depth climatology

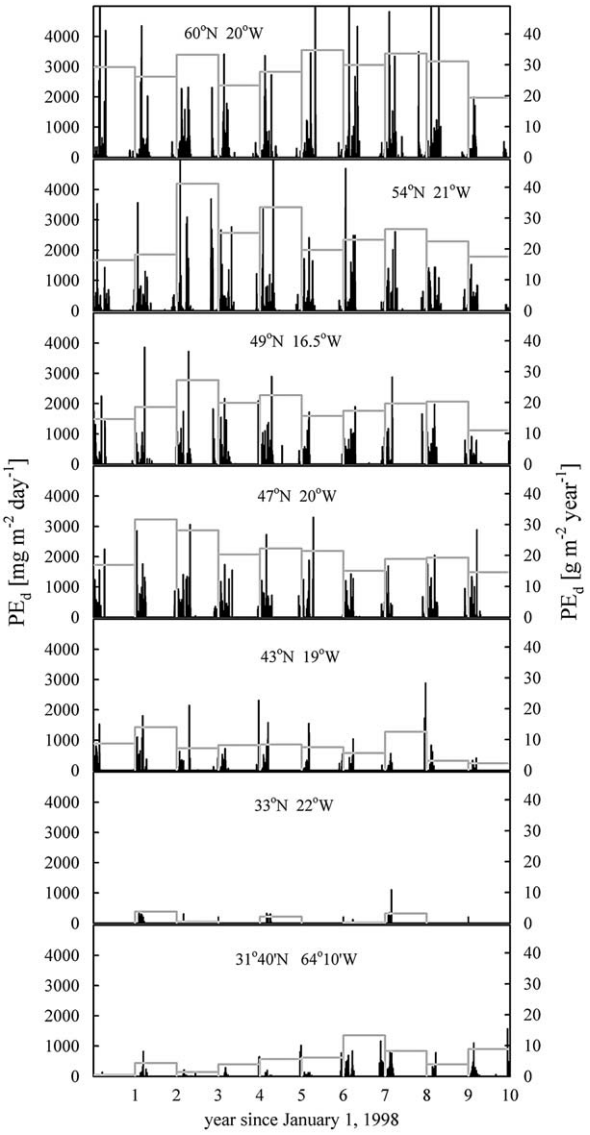

Fig. 6. Comparison of the model estimated 10-year time series of the diffusive POC flux at 200 m depth at seven sites in the North Atlantic. Daily time series of PE_d are shown as black solid lines and yearly totals are shown as gray histograms. The vertical scales on the left and right sides of Fig. 6 are for daily time series and yearly estimates of PE_d, respectively.

(from de Boyer Montégut et al., 2004) and the 10-year averaged surface POC concentration. Note, that PE_d is usually largest during early spring, when weakly stratified water allows for a development of deep mixing events associated with a passage of storm systems through the North Atlantic. These mixing events are responsible in our model for transporting POC particles below the 200 m depth.

In the northern North Atlantic (sites in the NARD and SARC provinces) surface POC concentrations are considerably larger in summer and early fall than in spring. For example the maximum POC values at 54°N range between 50 and 100 mg m^{-3} in March and between 120 and 150 mg m^{-3} in June–July (Fig. 7). In contrast to this seasonal trend in surface POC concentrations, the 10-year averaged PE_d is largest in February–May with strong short-lived flux peaks, while insignificantly low PE_d values are predicted for the summer season. On average some increase in PE_d also takes place in the late fall, which can be attributed to a considerable cooling of surface waters due to the seasonal increase in heat loss accompanied by stronger winds. Unfortunately, in the late fall and

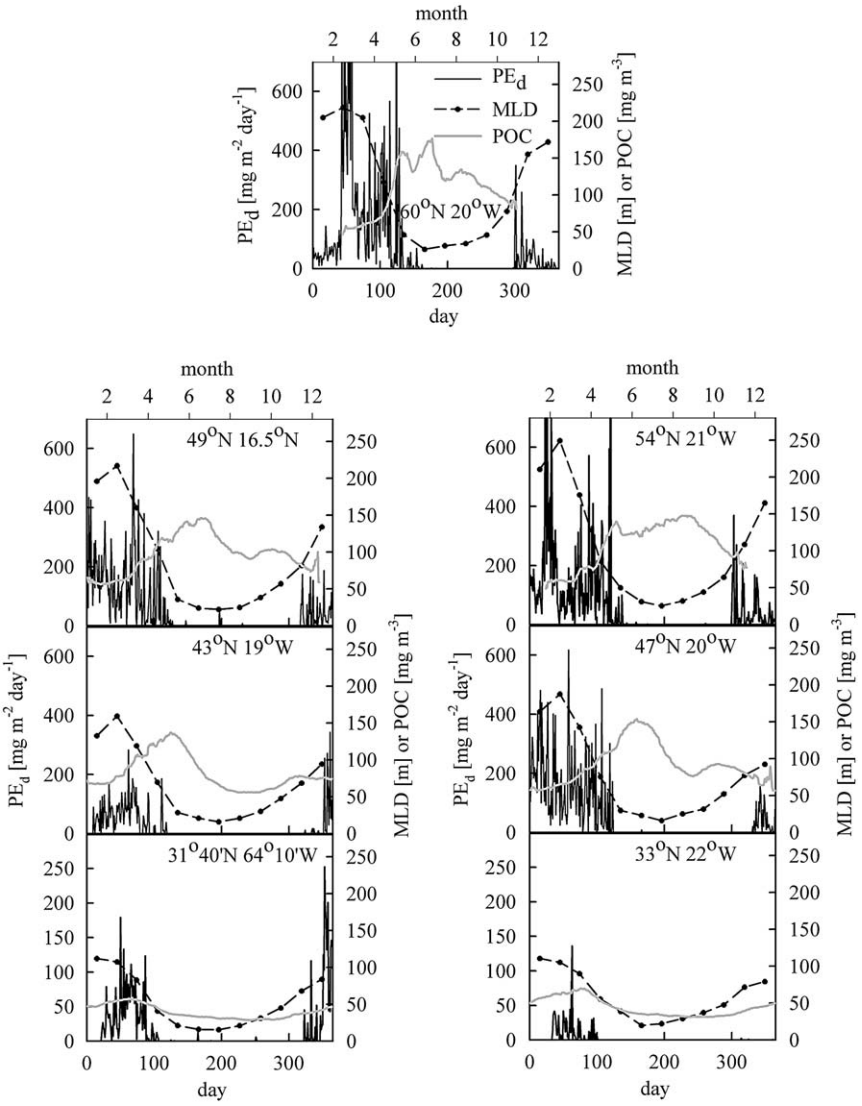

Fig. 7. Comparison of the 10-year average time series of the diffusive POC flux at 200 m (solid line), 10-year average time series of the surface POC concentration (gray line), and mixed layer depth (MLD) climatology (dashed line) at the seven sites in the North Atlantic.

winter, ocean color data are missing in the northern North Atlantic, due to frequent clouds. The severity of the problem increases towards polar regions, and the POC data are generally missing after day 300 at 60°N, after day 320 at 54°N, and after day 340 at 49°N (this is shown in Fig. 7, where the portions of the gray line indicating POC concentrations are missing). As noted in the methods sections, when ocean color data were missing, it was assumed in the model that there was no production of POC within the surface waters. This means that our estimates of PE_d in the late fall/winter in the northern North Atlantic are conservative and may somewhat underestimate the PE_d, if the assumption about null production is too restrictive.

As illustrated in Fig. 7, the seasonal cycle of POC concentration in the North Atlantic Subtropical Gyre is different than the seasonal cycle in the northern regions. Unlike in the northern North Atlantic, maximum POC concentrations in NAST-E and BATS sites are observed in winter, when the mixed layer is at its deepest. The POC concentrations and PE_d at these two sites are significantly smaller than at the other sites. In addition, the PE_d in NAST-E is smaller than at BATS, and the fall increase in PE_d is observed at BATS, while it is not present at NAST-E.

In Table 2 we compare ranges of regional estimates of the total POC export (PE) available from existing literature with our estimates of PE_d. Note that some of the published PE values listed in Table 2 are calculated from PP data (Dunne et al., 2007). Other PE estimates have been derived from POC fluxes measured with deep-water sediment traps and converted to PE through some assumptions (see Honjo et al., 2008). The intercomparisons of various sediment trap data are challenging, because such experiments usually differ in depth and duration of trap deployment, and sampling frequency. Typical results of sediment trap experiments represent discontinuous series of average flux rates corresponding to open–close bottle intervals of variable durations (several days or weeks). Therefore, sediment trap measurements do not resolve the relatively brief PE_d events modeled in this paper. Nevertheless it is still worthwhile to compare the annually averaged PE and PE_d estimates. The annual estimates of PE and PE_d summarized in Table 2 indicate that PE_d makes a significant contribution to total PE at all North Atlantic sites. In addition, the latitudinal trend in PE_d and PE is similar, with higher values in the north and lower values in the subtropical gyre regions.

The only site where it was possible to compare long-term time series from shallow water traps with our model output was BATS. These data are plotted in Fig. 8. There is a good temporal correspondence of the seasonal peaks in the PE measured by

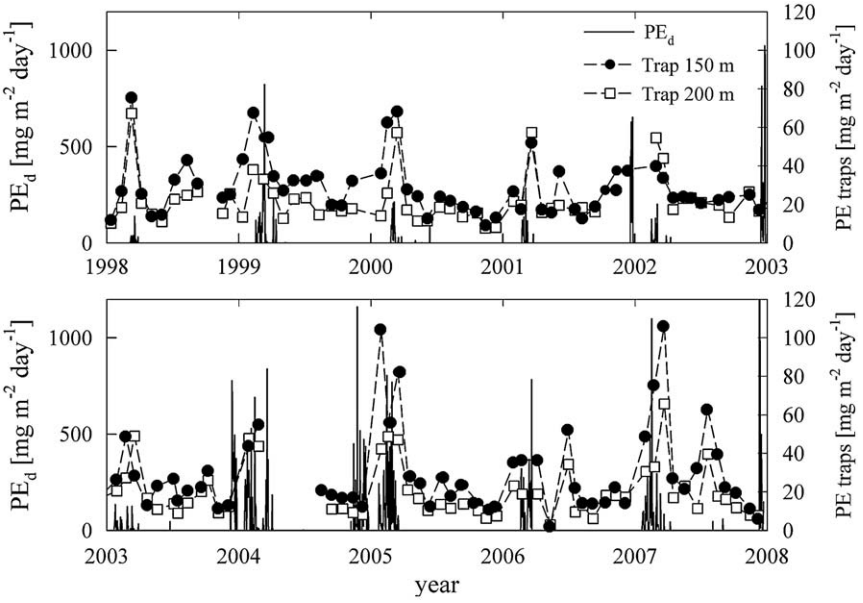

Fig. 8. Comparison of the 10-year time series of the diffusive POC flux at 200-m depth estimated with the model with time series of POC flux measured with sediment traps at BATS. Sediment trap data has been taken from (bats.bbsr.edu).

sediment traps and our estimates of PE_d, although the values of the peaks are much smaller in the sediment trap data records. There are at least three possible reasons for this difference. First, sediment traps at BATS averaged POC flux over 4–5 days, while PE_d was calculated with better temporal resolution (PE_d data in Fig. 8 are plotted as daily averages). Second, traps at BATS were only collecting data for 4–5 days every month, and most likely missed many of the short-lived episodic mixing events. Finally, traps are designed to collect particles transported by gravitational settling, but may miss a significant portion of particles transported by intense vertical mixing events.

Our results show a significant relationship between surface POC concentration and PE_d (Fig. 9). The coefficient of correlation r^2 between the 10-year averaged POC concentration and PE_d is higher than between annually averaged estimates of POC concentration and PE_d (compare Fig. 9a and b). If annually averaged data are considered separately for each study site the coefficient of correlation r^2 is always less than 0.3 (not shown). This suggests that the general trend of increase of PE_d with increasing surface POC concentration shown in Fig. 9 is more due to the latitudinal covariability of POC concentration and PE_d than to the temporal covariability.

Vertical export of marine particles is often modeled as a function of primary production (PP) in the ocean (e.g., Suess, 1980; Pace et al., 1987; Berger et al., 1987; Dunne et al., 2007). To examine the relationship between PE_d and PP as well as the relationship between PE_d and PE we have plotted in Figs. 10 and 11 our estimates of PE_d as a function of PP and PE, respectively. The PP and PE estimates for our study sites displayed in Figs. 10 and 11 were taken from Dunne et al. (2007). Data compared in Figs. 10a and b indicate that the correlation coefficient is lower for the annual estimates of PP and PE_d than for the multiyear averages (Fig. 10b). A similar result is found if we compare PE_d with PE estimates (Fig. 11). The interannual variability significantly increases the scatter of data points. As a consequence the correlation coefficient is lower for the relationship between annually averaged PE and PE_d estimates (Fig. 11a) than for the multiyear averages (Fig. 11b).

Our results are consistent with earlier findings based on analysis of in situ flux measurements. For example, at BATS there is a significant variability in the timing, duration and magnitude

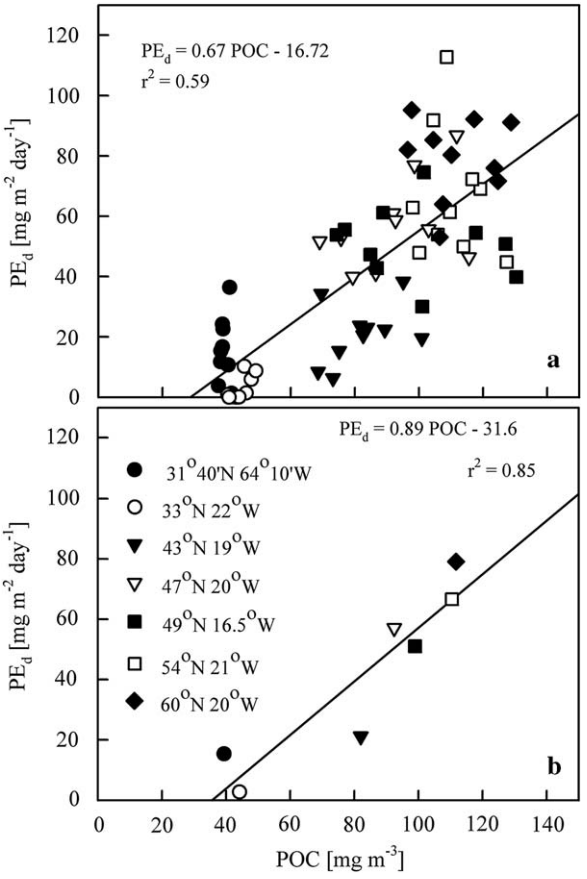

Fig. 9. (a) Yearly averaged estimates of the diffusive POC export plotted as a function of yearly averaged surface POC concentration. (b) The 10-year averaged estimates of the diffusive POC export plotted as a function of the 10-year averaged surface POC concentration.

of the seasonal peak flux, which cannot be explained by similar variability of PP (Deuser, 1986; Conte et al., 1998, 2001). In addition, the episodic high flux events, which are a persistent feature of the OFP record and are associated with a rapid transfer

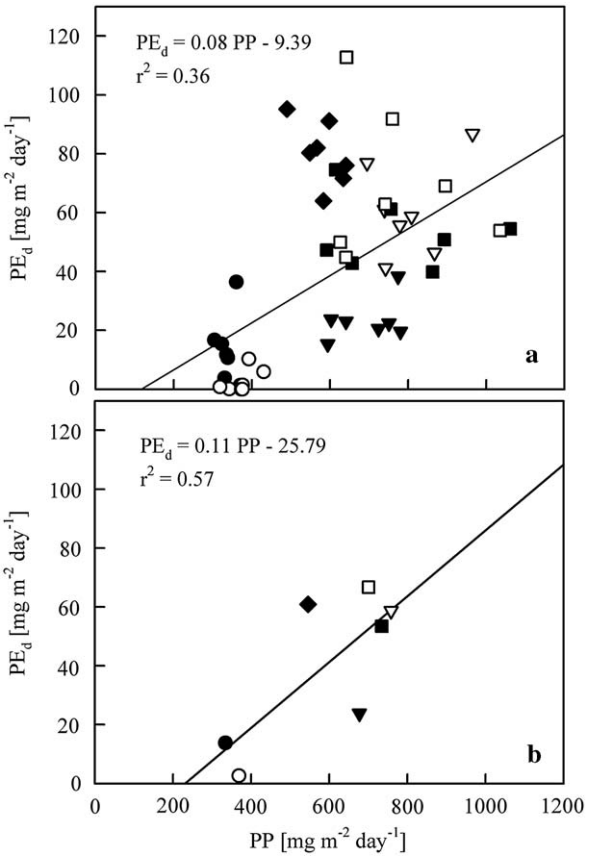

Fig. 10. (a) Yearly estimates in years 1998–2004 of the diffusive POC export plotted as a function of yearly averaged PP. PP estimates have been taken from Dunne et al. (2007). (b) Same as above, but the 7-year averaged estimates of diffusive POC export are plotted as a function of the 7-year averaged PP. Symbols are the same as in Fig. 9.

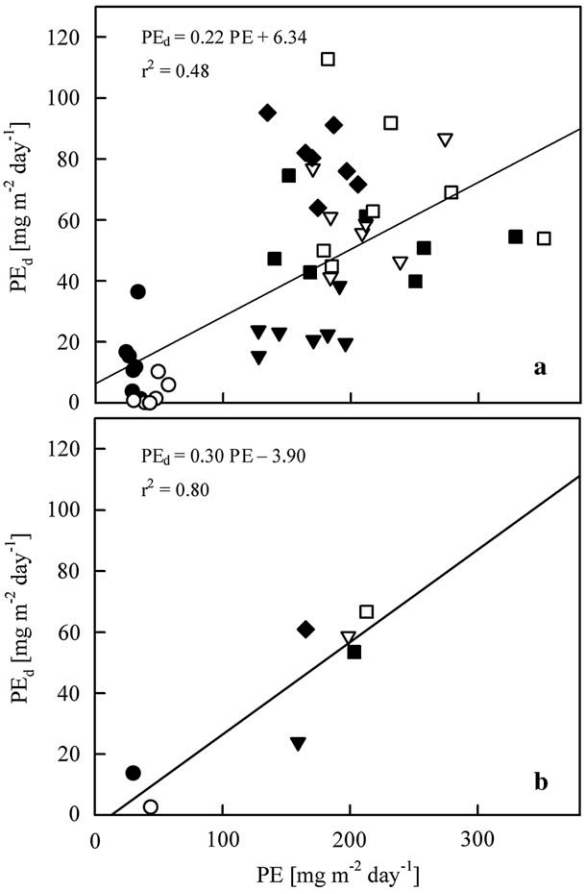

Fig. 11. (a) Yearly estimates of the diffusive POC export plotted as a function of yearly averaged total POC export, in years 1998–2004. Total POC export has been taken from Dunne et al. (2007). (b) Same as above, but the 7-year averaged estimates of diffusive POC export are plotted as a function of the 7-year averaged total POC export. Symbols are the same as in Fig. 9.

of fresh, biologically available organic carbon to the deep ocean, are decoupled from PP variability on the same time scale (Conte et al., 1998). Similar episodic events and a lack of a significant correlation between primary production and export production have been also reported in other sediment trap records (Newton et al., 1994; Fischer et al., 1996; Karl et al., 1996). Several possible explanations have been suggested for this decoupling (Karl et al., 1996), including enhanced retention of particles in surface waters during periods of high primary production that results in lower particle flux, intermittent production events in the lower euphotic zone missed by both satellite observations and the in situ PP sampling schedules, and heterogeneity in the source region of the trap and horizontal POC transport. Conte et al. (1998) noted that the high flux events at BATS are most frequent during times of low water column stability. This observation suggests that the observed high flux events may be forced physically by enhancement of upper ocean mixing and are similar to the PE_d flux component modeled in our paper. We propose that the relationship between atmospheric forcing of mixed layer dynamics and POC export should be examined more closely in the future as more in situ high-temporal resolution data from shallow water sediment traps become available.

The atmospheric influence on PE could be examined by assessing the relationship between PE and the rate of generation of turbulent kinetic energy (TKE_{RT}). As an example, Fig. 12 shows our estimates of PE_d plotted as a function of TKE_{RT} calculated using Eq. (5). The PE_d and TKE_{RT} data shown in Fig. 12 represent January–May averages (i.e. data were averaged over the time

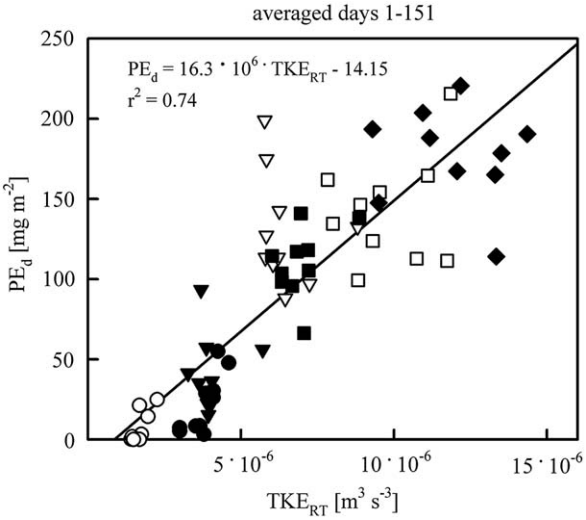

Fig. 12. The diffusive POC export plotted as a function of turbulent kinetic energy generation rate (TKE_{RT}). POC export and TKE_{RT} have been integrated for the time period of January–May (days 1–151 of each calendar year used in this study). Symbols are the same as in Fig. 9.

period when the modeled PE_d values were large, see Fig. 7). Importantly, there is a significant correlation between PE_d and TKE_{RT} shown in Fig. 12. In summary, our modeling results strongly support the notion that atmospheric forcing can exert a

considerable influence on PE. This happens through atmospherically controlled variability of PE_d, which can have a sizeable effect on total PE. This means that the atmospherically controlled PE_d variability can be one of the reasons why sediment traps receive at times strong, short-duration pulses of organic matter and why sediment trap derived estimates of particle flux are at times decoupled from PP.

5. Summary and conclusions

The quantification of regional and larger-scale estimates of POC export in the ocean from a limited number of in situ data has been a significant challenge in the past. In recent years, ocean color remote sensing has provided a powerful means for the study of ocean biogeochemistry and ecosystems over large spatial scales. Some quantities critical to the understanding of biogeochemical cycles and ecosystems are not directly accessible to satellite detection, but can be addressed through a combination of approaches. In this paper we have examined the diffusive vertical flux of POC using satellite-derived surface concentrations of POC combined with ocean physical model. This approach builds upon recent field-based evidence that surface POC concentration in the ocean can be assessed directly from satellite ocean color observations (see Stramski et al., 2008). Our method has the potential to provide long-term spatially resolved time series of diffusive POC flux, which might allow a detection of variability and trends in ocean carbon cycling.

The identification of the factors controlling the downward export of biogenic particles has received considerable attention for at least three decades (Berger et al., 1987; Suess, 1980; Boyd and Trull, 2007). Syntheses of our knowledge on this subject include global (e.g., Lutz et al., 2002; Dunne et al., 2007) and regional (e.g., Antia et al., 2001) analysis of particle export, global estimates of processes important to export such as PP (e.g., Behrenfeld and Falkowski, 1997), and comparisons between models and biogeochemical observations (Laws et al., 2000). These efforts have significantly increased our present understanding of the biological pump and the downward export of biogenic particles, but many unresolved questions remain.

POC particles present in the surface oceanic waters have low sinking velocities because their density is close to that of seawater. Traditionally, two processes have been attributed a major role for exporting POC. These are: transport associated with the zooplankton ecosystem, and transport by gravitational settling of biogenic aggregates ballasted by heavy biomineral and lithogenic particles (e.g., Honjo et al., 2008). Another potentially important mechanism for export of POC particles from surface waters is turbulent diffusion, in particular during energetic mixing episodes of surface waters in response to atmospheric forcing events. This mechanism did not receive much attention in the past, but our model calculations show that PE_d contributes significantly to total POC export from surface waters. Although turbulent diffusion cannot transport POC particles to great depths, it increases POC export and on average decreases the time necessary for particles to travel from surface water to intermediate depths. Our results also indicate that PE_d undergoes strong temporal variations. There are periods with insignificantly small PE_d flux, interrupted by strong, short sedimentation pulses. The efficiency of PE_d is generally greatest in early spring and late fall, when water column stability is weak and mixing events can penetrate to greater depths. Our preliminary estimates of PE_d derived in this paper indicate that there is also significant regional variability and annually averaged PE_d flux is greater in the northern North Atlantic than in the subtropical gyres.

At present it is difficult to fully verify our results with in situ data, because of the limited availability of direct measurements of POC export with high temporal resolution. Nevertheless, experimental data support our modeling results to some extent, because episodic high flux events consistent with modeled PE_d events have been observed in situ (e.g., Buesseler, 1998; Conte et al., 2001, 2003). In addition, a good temporal correspondence of the seasonal peaks in our estimates of PE_d and in the PE measured by shallow water sediment traps at BATS, and the fact that these peaks were not associated with concurrent peaks in PP also indirectly support our reasoning.

It is hard to predict what are the full consequences of PE_d events on the POC cycle in the ocean. One of the aspects that deserve special consideration is the fact that the mode and speed of vertical transport of particles determines the depth to which particles are exported and the degree to which they are remineralized in the water column. Bacterial solubilisation of particles is greatest in the surface waters and decreases with depth, which is an important factor controlling export and transformations of particles in the subsurface ocean. Therefore absence or presence of PE_d component in PE will most likely have an effect not only on the total value of PE, but also on the quality of the flux, and the depth to which the fresh, untransformed organic carbon can be transported. Note that the depth at which the material is remineralised or dissolves is important for carbon cycling, because it determines the time before it is once again able to contribute to ocean surface processes. Another aspect that is worth keeping in mind, is that an absence or presence of PE_d events may affect the determinations of the coefficient of attenuation of POC flux with depth (b) from in situ data, which is an important parameter in biogeochemical models. If the coefficient of attenuation of POC flux with depth is variable in time and regionally, we need to develop a good understanding of this variability and incorporate it into global biogeochemical models. In conclusion, our results strongly suggest that more direct determinations of POC flux with high temporal resolution and focused on the subsurface ocean where the flux changes most rapidly with depth are needed in order to develop an improved understanding of the issues raised by our modeling work.

Acknowledgments

Financial support for this research was provided by NASA Ocean Biology and Biogeochemistry Program (Grant NNX08AG02G). SeaWiFS data were made available by NASA's Goddard DAAC and the SeaWiFS Science Project. The National Centers for Environmental Prediction and National Center for Atmospheric Research (NCEP/NCAR) Reanalysis Project meteorological data were provided by NOAA-CIRES Climate Diagnostics Center. Sediment trap data were made available by the NSF-funded Bermuda Atlantic Time-series Study (BATS). I would like to thank C. de Boyer Montégut for mixed layer depth climatology data and John Dunne for PP and PE estimates. I am grateful to two anonymous reviewers and Dr. M.P Bacon for very useful remarks and suggestions.

References

Anderson, L.G., Drange, H., Chierici, M., Fransson, A., Johannessen, T., Skjelvan, I., Rey, F., 2000. Annual carbon fluxes in the upper Greenland Sea based on measurements and a box-model approach. Tellus 52B, 1013–1024.

Antia, A.N., Koeve, W., Fischer, G., Blanz, T., Schulz-Bull, D., Scholten, J., Neuer, S., Kremling, K., Kuss, J., Peinert, R., Hebbeln, D., Bathmann, U., Conte, M., Fehner, U., Zeitzschel, 2001. Basin-wide particulate carbon flux in the Atlantic Ocean: regional export patterns and potential for atmospheric CO_2 sequestration. Global Biogeochemical Cycles 15, 845–862.

Antoine, D., Andre, J.-M., Morel, A., 1996. Oceanic primary production 2. Estimation at global scale from satellite (coastal zone color scanner) chlorophyll. Global Biogeochemical Cycles 10, 57–69.
Behrenfeld, M.J., Boss, E., Siegel, D.A., Shea, D.M., 2005. Carbon-based ocean productivity and phytoplankton physiology from space. Global Biogeochemical Cycles 19, GB1006, doi:10.1029/2004GB002299.
Behrenfeld, M.J., Falkowski, P.G., 1997. Photosynthetic rates derived from satellite-based chlorophyll concentration. Limnology and Oceanography 42, 1–20.
Berelson, W., 2001. The flux of particulate organic carbon into the ocean interior: a comparison of four JGOFS regional studies. Oceanography 14, 59–67.
Berger, W.H., Fischer, K., Lai, C., Wu, G., 1987. Ocean carbon flux: Global maps of primary production and export production. In: Agegian, C., (Ed.), Biogeochemical Cycling and Fluxes between the Deep Euphotic Zone and Other Oceanic Realms. SIO Ref. 87-30, pp. 1–44, University of California, San Diego, Scripps Institute of Oceanography, La Jolla, California.
Blumberg, Mellor, G.L., 1983. Diagnostic and prognostic numerical circulation studies of the South California Bight. Journal of Geophysical Research 88, 4579–4592.
Boyd, P.W., Stevens, C.L., 2002. Modelling particle transformations and the downward organic carbon flux in the NE Atlantic Ocean. Progress in Oceanography 52, 1–29.
Boyd, P.W., Trull, T.W., 2007. Understanding the export of biogenic particles in oceanic waters: is there consensus? Progress in Oceanography 72, 276–312.
Buesseler, K.O., 1998. The decoupling of production and particulate export in the surface ocean. Global Biogeochemical Cycles 12, 297–310.
Buesseler, K.O., Bacon, M.P., Cochran, J.K., Livingston, H.D., 1992. Carbon and nitrogen export during the JGOFS North Atlantic bloom experiment estimated from ^{234}Th:^{238}U disequilibria. Deep-Sea Research Part A 39, 1115–1137.
Buesseler, K.O., Andrews, J.A., Hartman, M.C., Belastock, R., Chai, F., 1995. Regional estimates of the export flux of particulate organic carbon derived from ^{234}Th during the JGOFS EqPac program. Deep-Sea Research II 42, 777–804.
Carr, M.-E., 2002. Estimation of potential productivity in Eastern Boundary Currents using remote sensing. Deep Sea Research II 49, 59–80.
Campbell, J.W., Blaisdell, J.M., Darzi, M., 1995. Level-3 SeaWiFS data products: spatial and temporal binning algorithms. SeaWiFS Technical Report Series 32, 73.
Conte, M.H., Weber, J.C., Ralph, N., 1998. Episodic particle flux in the deep Sargasso Sea: an organic geochemical assessment. Deep-Sea Research I 45, 1819–1841.
Conte, M.H., Ralph, N., Ross, E.H., 2001. Seasonal and interannual variability in deep ocean particle fluxes at the Oceanic Flux Program (OFP)/Bermuda Atlantic Time Series (BATS) site in the western Sargasso Sea near Bermuda. Deep-Sea Research II 48, 1471–1505.
Conte, M.H., Dickey, T.D., Weber, J.C., Johnson, R.J., Knap, A.H., 2003. Transient physical forcing of pulsed export of bioreactive material to the deep Sargasso Sea. Deep-Sea Research Part I 50, 1157–1187.
de Boyer Montégut, C., Madec, G., Fischer, A.S., Lazar, A., Iudicone, D., 2004. Mixed layer depth over the global ocean: an examination of profile data and a profile-based climatology. Journal of Geophysical Research 109, C12003, doi:10.1029/2004JC002378.
Dickey, T., Marra, J., Stramska, M., Langdon, C., Granata, T., Weller, R., Plueddemann, A., Yoder, J., 1994. Bio-optical and physical variability in the sub-Arctic North Atlantic Ocean during spring of 1989. Journal of Geophysical Research 99, 22541–22556.
Deuser, W.G., 1986. Seasonal and interannual variations in deep-water particle fluxes in the Sargasso Sea. Nature 283, 364–365.
Ducklow, H.W., Steinberg, D.K., Buesseler, K.O., 2001. Upper ocean carbon export and the biological pump. Oceanography 14 (4), 50–58.
Dugdale, R.C., Goering, J.J., 1967. Uptake of new and regenerated forms of nitrogen in primary productivity. Limnology and Oceanography 12, 196–206.
Dunne, J., Sarmiento, J.L., Gnanadesikan, A., 2007. A synthesis of global particle export from the surface ocean and cycling through ocean interior and seafloor. Global Biogeochemical Cycles, 21.
Edwards, A.M., 2001. Adding detritus to a nutrient-phytoplankton-zooplankton model: a dynamical system approach. Journal of Plankton Research 23, 389–413.
Eppley, R.W., 1989. New production, history, methods, problems. In: Berger, W.H., Smetacek, V.S., Wefer, G. (Eds.), Productivity of the Ocean: Present and Past. Wiley & Sons, New York.
Eppley, R.W., Peterson, B.J., 1979. Particulate organic matter flux and planktonic new production in the deep ocean. Nature 282, 677–680.
Fasham, M.J.R., Ducklow, H.W., McKelvie, S.M., 1990. A nitrogen-based model of plankton dynamics in the oceanic mixed layer. Journal of Marine Research 48, 591–639.
Fischer, G., Neuer, S., Krause, G., Wefer, G., 1996. Short-term sedimentation pulses recorded with a fluorescence sensor and sediment traps in 900 m water depth in the Canary Basin. Limnology and Oceanography 41, 1354–1359.
Follows, M., Dutkiewicz, S., 2002. Meteorological modulation of the North Atlantic spring bloom. Deep-Sea Research II 49, 321–344.
Guieu, C., Roy-Barman, M., Leblond, N., Jeandel, C., Souhaut, M., Le Cann, B., Dufour, A., Bournot, C., 2005. Vertical particle flux in the northeast Atlantic Ocean (POMME experiment). Journal of Geophysical Research 110, C07S18, doi:10.1029/2004JC002672.
Glover, D.M., Brewer, P.G., 1988. Estimates of wintertime mixed layer nutrient concentrations in the North Atlantic. Deep-Sea Research Part A 35 (9), 1525–1546.
Gordon, H.R., Wang, M., 1994. Retrieval of water-leaving radiance and aerosol optical thickness over the oceans with SeaWiFS: a preliminary algorithm. Applied Optics 33, 443–452.
Honjo, S., Manganini, S.J., 1987. Particle Fluxes, North-Eastern Nordic Seas: 1983–1986. Nordic Seas Sedimentation Data File, vol. 1. WHOI Technical Report 87-17, Woods Hole Oceanographic Institution, Woods Hole.
Honjo, S., Manganini, S.J., Krishfield, R.A., Francois, R., 2008. Particulate organic carbon fluxes to the ocean interior and factors controlling the biological pump: a synthesis of global sediment trap programs since 1983. Progress in Oceanography 76, 217–285.
Huisman, J., van Oostveen, P., Weissing, F.J., 1999. Critical depth and critical turbulence: two different mechanism for the development of phytoplankton blooms. Limnology and Oceanography 44, 1781–1788.
IOCCG, 2004. Guide to the Creation and Use of Ocean-Colour, Level-3, Binned Data Products. Antoine, D., (ed.), Reports of the International Ocean-Colour Coordinating Group. No. 4, IOCCG, Dartmouth, Canada.
Jerlov, N.G., 1968. Optical Oceanography. Elsevier, Amsterdam 194pp.
Kantha, L.H., 2004. A general ecosystem model for applications to primary productivity and carbon cycle studies in the global oceans. Ocean Modelling 6, 285–334.
Karl, D.M., Christian, J.R., Dore, J.E., Hebel, D.V., Letelier, R.M., Tupas, L.M., Winn, C.D., 1996. Seasonal and interannual variability in primary production and particle flux at Station ALOHA. Deep-Sea Research II 43, 539–568.
Kraus, E.B., Turner, J.S., 1967. A one-dimensional model of the seasonal thermocline, part II: the general theory and its consequences. Tellus 19, 98–106.
Kraus, E.B., Bleck, R., Hanson, H.P., 1988. The inclusion of a surface mixed layer in a large-scale circulation model. In: Nihoul, J.C.J., Jamart, B.M. (Eds.), Small Scale Turbulence and Mixing in the Ocean. Elsevier, Amsterdam, pp. 51–62.
Lampitt, R.S., Bett, B.J., Kiriakoulakis, K., Popova, E.E., Ragueneau, O., Vangriesheim, A., Wolff, G.A., 2001. Material supply to the abyssal seafloor in the Northeast Atlantic. Progress in Oceanography 50 (1–4), 27–63.
Laws, E.A., Falkowski, P.G., Smith, W.O., Ducklow, H., McCarthy, J.J., 2000. Temperature effects on export production in the open ocean. Global Biogeochemical Cycles 14, 1231–1246.
Legendre, L., Rivkin, R.B., 2002. Fluxes of carbon in the upper ocean: regulation by food-web control nodes. Marine Ecology Progress Series 242, 95–109.
Levy, M., Lehahn, Y., Andre, J.-M., Memery, L., Loisel, H., Heifetz, E., 2005. Production regimes in the northeast Atlantic: a study based on Sea-viewing Wide Field-of-view Sensor (SeaWiFS) chlorophyll and ocean general circulation model mixed layer depth. Journal of Geophysical Research 110, C07S10, doi:10.1029/2004JC002771.
Lima, I.D., Doney, S.C., 2004. A three-dimensional, multinutrient, and size-structured ecosystem model for the North Atlantic. Global Biogeochemical Cycles 18, GB3019, doi:10.1029/2003GB002146.
Lomas, M.W., Bates, N.R., 2004. Potential controls on interannual partitioning of organic carbon during the winter/spring phytoplankton bloom at the Bermuda Atlantic time-series (BATS) site. Deep-Sea Research I 51, 1619–1636.
Longhurst, A., 1998. Ecological Geography of the Sea. Academic Press, New York, pp. 398.
Lutz, M., Dunbar, R., Caldeira, K., 2002. Regional variability in the vertical flux of particulate organic carbon in the ocean interior. Global Biogeochemical Cycles 16, 1037, doi:10.1029/2000GB001383.
Martin, J.H., Fitzwater, S.E., Gordon, R.M., Hunter, C.N., Tanner, S., 1993. Iron, primary production, and carbon-nitrogen flux studies during the JGOFS North Atlantic Bloom Experiment. Deep-Sea Research II 40, 115–134.
Marra, J., Ho, C., 1993. Initiation of the spring bloom in the northeast Atlantic (47°N, 20°W): a numerical simulation. Deep-Sea Research II 40, 55–73.
Marra, J., Ho, C., Trees, C.C., 2003. An alternative algorithm for the calculation of primary productivity from remote sensing data. LDEO Tech. Rep. LDEO-2003-1, Lamont Doherty Earth Obs., Palisades, NY.
Mellor, G.L., Yamada, T., 1974. A hierarchy of turbulence closure models for planetary boundary layers. Journal of Atmospheric Science 31, 1791–1806.
Mellor, G.L., Yamada, T., 1982. Development of a turbulence closure model for geophysical problems. Reviews in Geophysics and Space Physics 20, 851–857.
Mellor, G.L., 2004. Users Guide for a three-dimensional, primitive equation numerical ocean model. Available on the Princeton Ocean Model (POM) web site, rev. 2004. (http://www.aos.princetion.edu/WWPUBLIC/htdocs.pom/).
Memery, L., Reverdin, G., Paillet, J., Oschlies, A., 2005. Introduction to the POMME special section: thermocline ventilation and biogeochemical tracer distribution in the northeast Atlantic Ocean and impact of mesoscale dynamics. Journal of Geophysical Research 110, C07S01, doi:10.1029/2005JC002976.
Michaels, A.F., Bates, N.R., Buesseler, K.O., Carlson, C.A., Knap, A.H., 1994. Carbon-cycle imbalances in the Sargasso Sea. Nature 372, 537–539.
Michaels, A.F., Knap, A.H., 1996. Overview of the US JGOFS Bermuda Atlantic Time-series Study and the Hydrostation S program. Deep-Sea Research II 43, 157–198.
Mobley, C.D., 1994. Light and Water: Radiative Transfer in Natural Waters. Academic Press, New York.
Neuer, S., Davenport, B., Freudenthal, T., Wefer, G., Llina′s, O., Rueda, M.-J., Steinberg, D.K., Karl, D.M., 2002. Differences in the biological carbon pump at three subtropical ocean sites. Geophysical Research Letters, 29, doi:10.1029/2002GL01539.
Neuer, S., Cianca, A., Helmke, P., Freudenthal, T., Davenport, R., Meggers, H., Knoll, M., Santana-Casiano, J.M., Gonzalez-Davila, M., Rueda, M.-J., Llinas, O., 2007. Biogeochemistry and hydrography in the eastern subtropical North Atlantic gyre. Results from the European time-series station ESTO. Progress in Oceanography 72, 1–29.

Newton, P.P., Lampitt, R.S., Jickells, T.D., King, P., Boutle, C., 1994. Temporal and spatial variability of biogenic particle fluxes during JGOFS northeast Atlantic process studies at 47°N 20°W. Deep-Sea Research I 41, 1617–1642.

Niiler, P.P., Kraus, E.B., 1977. One-dimensional models of the upper ocean. In: Kraus, E.B. (Ed.), Modelling and Predictions of the Upper Layers of the Ocean. Pergamon, Oxford, pp. 143–172.

O'Reilly, J.E., Maritorena, S., Mitchell, B.G., Siegel, D.A., Carder, K.L., Garver, S.A., Kahru, M., McClain, C.R., 1998. Ocean color chlorophyll algorithms for SeaWiFS. Journal of Geophysical Research 103, 24937–24953.

O'Reilly, J.E., Maritorena, S., Siegel, D.A., O'Brien, M.C., Toole, D., Mitchell, B.G., Kahru, M., Chavez, F.P., Strutton, P., Cota, G.F., Hooker, S.B., McClain, C.R., Carder, K.L., Müller-Karger, F., Harding, L., Magnuson, A., Phinney, D., Moore, G.F., Aiken, J., Arrigo, K.R., Letelier, R., Culver, M., 2000. Ocean color chlorophyll a algorithms for SeaWiFS, OC2 and OC4: Version 4, NASA Tech. Memo, 2000-206892, vol. 11, 9–27.

Pace, M.L., Knauer, G.A., Karl, D.M., Martin, J.H., 1987. Primary production, new production and vertical flux in the eastern Pacific. Nature 325, 803–804.

Paulson, C.A., Simpson, J.J., 1977. Irradiance measurements in the upper ocean. Journal of Physical Oceanography 7, 952–956.

Patsch, J., Kuhn, W., Radch, G., Santana, J.M., Casiano, Gonzalez Davila, M., Neuer, S., Freudenthal, T., Llinas, O., 2002. Interannual variability of carbon fluxes at the North Atlantic Station ESTOC. Deep-Sea Research II 49, 253–288.

Plueddemann, A., Weller, R., Stramska, M., Dickey, T., Marra, J., 1995. The vertical structure of the upper ocean during the marine light—mixed layer experiment. Journal of Geophysical Research 100, 6621–6632.

Schlitzer, R., 2004. Export production in the Equatorial and North Pacific derived from dissolved oxygen, nutrient and carbon data. Journal of Oceanography 60 (1), 53–62.

Schlitzer, R., Usbeck, R., Fischer, G., 2003. Inverse modeling of particulate organic carbon fluxes in the South Atlantic. In: The South Atlantic in the Late Quaternary: Reconstruction of Material Budgets and Current Systems. Springer-Verlag, Berlin, Heidelberg, New York, Tokyo, pp. 1–19.

Scholten, J.C., Fietzke, J., Vogler, S., Loeff, M.M.R., Mangini, A., Koeve, W., Waniek, J., Stoffers, P., Antia, A., Kuss, J., 2001. Trapping efficiencies of sediment traps form the deep eastern North Atlantic: the ^{230}Th calibration. Deep Sea Research Part II 48, 2383–2408.

Siegel, D.A., Deuser, W.G., 1997. Trajectories of sinking particles in the Sargasso Sea: modeling of statistical funnels above deep-ocean sediment traps. Deep-Sea Research I 44, 1519–1541.

Siegel, D.A., Fields, E., Buesseler, K.O., 2008. A bottom-up view of the biological pump: modeling source funnels above ocean sediment traps. Deep-Sea Research I 55, 108–127.

Steinberg, D.K., Carlson, C.A., Bates, N.R., Johnson, R.J., Michaels, A.F., Knap, A.H., 2001. Overview of the US JGOFS Bermuda Atlantic Time-series Study (BATS): a decade-scale look at ocean biology and biogeochemistry. Deep Sea Research II 48, 1405–1447.

Stramska, M., 2009. Particulate organic carbon in the global ocean derived from SeaWiFS ocean color. Deep-Sea Research I 56, 1459–1470.

Stramska, M., Dickey, T.D., Marra, J., Plueddemann, A., Langdon, C., Weller, R., 1995. Bio-optical variability associated with phytoplankton dynamics in the North Atlantic Ocean during spring and summer of 1991. Journal of Geophysical Research 100, 6605–6619.

Stramski, D., Reynolds, R.A., Babin, M., Kaczmarek, S., Lewis, M.R., Röttgers, R., Sciandra, A., Stramska, M., Twardowski, M.S., Franz, B.A., Claustre, H., 2008. Relationships between the surface concentration of particulate organic carbon and optical properties in the eastern South Pacific and eastern Atlantic Oceans. Biogeosciences 5, 171–201.

Suess, E., 1980. Particulate organic carbon flux in the oceans-surface productivity and oxygen utilization. Nature 288, 260–263.

Usbeck, R., Schlitzer, R., Fischer, G., Wefer, G., 2003. Particle fluxes in the ocean: comparison of sediment trap data with results from inverse modeling. Journal of Marine Systems 39, 167–182.

Waniek, J., Schulz-Bull, D.E., Blanz, T., Prien, R., Oschlies, A., Muller, T.J., 2005a. Interannual variability of deep water particle flux in relation to production and lateral sources in the northeast Atlantic. Deep-Sea Research Part I 52, 33–50.

Waniek, J., Schulz-Bull, D.E., Kuss, J., Blanz, T., 2005b. Long time series of deep water particle flux in three biogeochemical provinces of the northeast Atlantic. Journal of Marine Systems 56, 391–415.